

# Elastic and inelastic scattering components in the angular intensity distribution of He scattered from graphite

June Pyo Oh, Takahiro Kondo\*, Daigo Hatake and Junji Nakamura

Institute of Frontier Science, University of Tsukuba, 1-1-1 Tennoudai, Tsukuba, Ibaraki 305-8573, Japan

\*corresponding author: [takahiro@ims.tsukuba.ac.jp](mailto:takahiro@ims.tsukuba.ac.jp)

## Abstract

The angular intensity distribution of thermal energy He beam scattered from highly oriented pyrolytic graphite (HOPG) surface has been measured by means of supersonic molecular beam scattering technique in the wide surface temperature range. To separate the elastic and inelastic scattering components, simple analysis method has been developed by applying the classical binary collision theory of the hard cube model (HCM). From the extracted elastic scattering component in the scattering distribution, the Debye temperature of the HOPG surface has been derived as  $590 \pm 30$  K. On the basis of the HCM analysis for the extracted inelastic scattering components of He beam, the effective mass for the HOPG surface has been found to be 72 u (six carbon atoms).

## Keywords

Highly oriented pyrolytic graphite (HOPG); Debye temperature; Effective mass; Molecular beam; Hard cube model

## 1. Introduction

Scattering of low energy He beam is one of the most fundamental gas-surface interactions [1-9]. It consists of elastic, quasi-elastic and inelastic scattering such as single phonon and multi-phonon scatterings. The dominant scattering channel is determined by the collision parameter of He with the surface such as surface temperature, incident translational energy of He, incident angle and the property of the surface. In the case of the graphite (0001) surface, for example, inelastic scattering component is expected as a dominant channel because the graphite consists of soft graphene layer composed by the light carbon atoms. To accurately analyze the each scattering component of He, clear distinction of each component from experimentally measured scattering results is indispensable. In this work, we have proposed a new method to extract elastic and inelastic scattering components by applying the simple classical binary collision model of the hard cube model [10].

Elastic scattering of low energy He beam has been mainly used to analyze the structure of the outermost surface of the solid [2, 4, 7]. The advantage of the measurement is that the surface structure of the metal, semiconductor, insulator and even molecular layer can be sensitively measured without any perturbation of the surface owing to the neutral charge and low kinetic energy of the He beam. The measurement has also revealed quantized potential well of the gas-surface interaction through the observation of the selective-adsorption, so-called resonant scattering. Rich surface information such as surface Debye temperature, morphological change, diffusion behavior of adspecies, and phase transition can also be derived by monitoring the intensity of the elastic scattering of He as a function of surface temperature. The sensitivity of the He for the detection of the morphological change is known to be extremely high owing to the large scattering cross section ( $\sim 100 \text{ \AA}^2$ ) of the low energy He atom towards adsorbed molecule or defect (the object which causes the modulation of the attractive potential of the surface). That is, the number of surface adspecies at coverage around 0.001 can be determined [3]. The measurement of the thermal energy He atom scattering (TEAS) has thus been widely used as one of the most powerful tools of the surface science study [3, 4, 7].

On the other hand, single-phonon scattering in the inelastic scattering component derived from the time-of-flight measurement has been used to construct the complete surface phonon dispersion curves [4-7]. Time-of-flight measurements have also unveiled the vibrational energy of the hindered-translational mode of the adsorbed molecule on the surface [6-9]. The vibrational energy of this mode is known to be quite difficult to measure with the typical vibrational spectroscopy methods such as infrared reflection absorption spectroscopy and high-resolution electron energy loss spectroscopy due to their selection rules in the measurement [11].

Contrary to the elastic, single-phonon and single-vibrational mode scattering components,

the multi-phonon (and electron-hole pair excitation) scattering component of the He beam has not been used to analyze the gas-surface interaction mainly because of its complicated phenomena to represent by the quantum mechanical description. Most of the He scattering works have thus been conducted at low surface temperature and very low incident kinetic energy of He in order to suppress the component of the multi-phonon scattering. In the multi-phonon scattering component of He, however, several important information are included such as effective mass of the surface interacting with He, trapping probability of He, energy dissipation process of He by the collision and so on. Manson has already established sophisticated analytical description to represent such an inelastic component of He by the classical scattering theory [12-14]. The analysis of the multi-phonon scattering by this theory derive the corrugation degree of the interaction potential between He and the surface even at the condition with higher He incident energy and surface temperature. The theory is applicable for the wide scattering conditions even for the scattering at the soft material surface such as liquid surface because of the inclusion of the multiple collision scatterings as well as single collision scattering. For the analysis by this theory, experimentally observed final translational energy and angular intensity distributions are at least required as well as a parameter of  $v_R$ , a weighted average of sound velocities parallel to the surface, which, in principle, can be calculated if the phonon spectral density is known [15].

In this work, we have first measured the angular intensity distributions of thermal energy He beam scattered from the highly oriented pyrolytic graphite (HOPG) surface at wide surface temperature range. We have then analyzed our experimental results by newly developed simple method. The HOPG surface is selected as a test sample because of the following three reasons; 1) the inelastic scattering of He is expected as a dominant scattering channel due to light mass of the surface atom, 2) several results for the elastic and single-phonon He scattering from graphite are available in the literatures [16-22], so that we can check the validity of the usage of our result of the extracted elastic component and 3) the same surface condition can be kept during the experiment because the surface is chemically stable. To separate the elastic and inelastic scattering components, we have applied the simple classical binary collision theory of the hard cube model (HCM) proposed by Logan and Stickney [10]. The model has been used in the field of molecular (or heavier atomic) beam scattering [23-25], to delineate trends in multi-phonon scattering of atoms and molecules from flat metal surfaces. The advantage of the model is its simplicity. It requires only one parameter of the effective surface mass to analytically calculate the multi-phonon scattering.

## 2. Experimental

The experimental apparatus used in this work has already been described elsewhere [26,

27]. The apparatus consists of five stainless-steel chambers. Each chamber is independently pumped to ultrahigh vacuum (UHV). A supersonic He beam is generated by free-jet expansion from a pinhole of a cylindrical nozzle and skimmed using a conical skimmer. The diameter of the nozzle pinhole is set to 0.05 mm. The translational energy of the He beam is experimentally identified by the time-of-flight technique. Fig. 1 shows the time-of-flight spectrum of the thermal energy He beam used in this work. The incident translational energy and  $\Delta E/E$  of the beam have been estimated as 63 meV (wave vector  $k = 11 \text{ \AA}^{-1}$ ) and 0.27, respectively [26].

The sample surface of highly oriented pyrolytic graphite (HOPG, NT-MDT Co., Russia, 12 mm  $\times$  12 mm  $\times$  1.5 mm, grade ZYA) was cleaved in air by adhesive tape and then put into a UHV chamber. The HOPG sample was mounted to a sample holder which can be cooled down to 90 K by a cryogenic refrigerator head (Iwatani CryoMini S050) and can be heated by the infrared radiation from a hot W filament placed close to the back side of the HOPG sample. The surface temperature of HOPG was measured by a type-K thermocouple attached on the edge of the sample by a Ta clamp. Prior to the experiment, the HOPG sample was annealed at 900 K in UHV for 5 min in order to clean the surface.

The angular intensity distribution measurement is carried out for scattered He atoms from the surface by rotating the sample along the axis perpendicular to the beam line with an accuracy of  $\pm 0.1^\circ$ . Throughout the present study, both incident and scattering angles are defined with respect to the surface normal direction. The sum of the incident and scattering angles has been fixed at  $90^\circ$ .

### 3. Result and Discussions

The angular intensity distribution of He scattered from the HOPG surface at 150 K is shown in Fig. 2. Despite the low surface temperature, non-negligible inelastic scattering components appear as broad distribution around elastic scattering component at the scattering angle of  $\theta_f = 45^\circ$ . The broad distribution is also caused by the irregularities of the surface such as step, defect and domain boundary. There are, however, two distinct diffraction peaks at around  $35^\circ$  and  $55^\circ$  as first diffraction peaks of (1, 0) and (-1, 0), respectively, suggesting that the flat area of the HOPG surface consists of uniform lattice arrangement. The intensity ratio of the (1, 0) and (0, 0) diffraction peaks correspond to be around the middle between those of typical insulator and metal surfaces [1-4]. The corrugation amplitude of the outermost electronic clouds of HOPG is thus considered to be somehow larger than that of the metal surface but it is not as much as that of the insulator surface as previously observed by the He scattering from the single crystal graphite (0001) surface [16, 21]. From diffraction peaks in Fig. 2, it is difficult to accurately estimate the surface lattice parameter directly due to the broad inelastic scattering background.

As shown in Fig. 3, the angular intensity distribution of He is significantly depending on the surface temperature. With the increase of the surface temperature, the elastic scattering component at  $\theta_f = 45^\circ$  decreases due to the Debye-Waller effect [2, 4]. It is again difficult to accurately estimate the surface Debye temperature from the dependence of the specular He intensity on the surface temperature due to the non-negligible inelastic scattering background. At the surface temperature of 400 K, the elastic peak can not clearly distinguish from background inelastic scattering component. The temperature dependence of the angular intensity distribution in Fig. 3 is therefore considered to show the transition of the scattering event from quantum mechanical scattering to the classical mechanical scattering of He.

In the following section, analysis method and analyzed results of distinction between elastic and inelastic scattering components are presented at first. The details of each elastic and inelastic scattering components are then discussed in detail.

### 3.1 Separation into elastic and inelastic scattering components

To make a sharp distinction between elastic and inelastic scattering components, the following analysis method is applied to the several angular intensity distributions of He from HOPG obtained at different surface temperatures as shown in Fig. 3. Equation used for the fitting analysis is described as:

$$I(\theta_f, T_s) = \alpha_{HCM} \times (\text{Elastic scattering component}) + \beta_{HCM} \times I_{HCM} \quad (1),$$

where  $I$  is the intensity of the scattered He beam at the scattering angle of  $\theta_f$ ,  $T_s$  is the surface temperature,  $\alpha_g$ ,  $\beta_g$ ,  $\alpha_{HCM}$  and  $\beta_{HCM}$  are the component factors used as the fitting parameter. The elastic scattering component is represented by the simple Gaussian function, where the width of the distribution ( $\sim 1^\circ$ ) is larger than the angular resolution of the apparatus ( $0.1^\circ$ ) [26], possibly due to the inhomogeneous structure of the HOPG surface. The inelastic scattering component is represented by the hard cube model calculation as  $I_{HCM}$ , where the parameters for the calculation are fixed by the experimental conditions except for the effective surface mass and the component factors. Therefore, in the process of the fitting analysis of the experimental results with equation (1),  $\alpha_{HCM}$ ,  $\beta_{HCM}$  and  $M$  are varied as fitting parameters.

The hard cube model used for the analysis rests on the assumption that the tangential component of momentum of the atom is conserved during the single collision event with the surface. The perpendicular component of momentum of the atom is altered via an impulsive hard wall collision with a vibrating cube [10]. The hard cube model has been remarkably successful in correlating experimental data and predicting their dependence on mass and surface temperature especially for the rare gas scattering from flat metal surface [28]. The  $I_{HCM}$  is explicitly described [10] as:

$$I_{HCM} = \frac{1}{u_{i\perp}} \int_0^\infty (\cos\theta_i + B_1) B_2 u_i^2 F_i(u_i) G_i(B_1 u_i) du_i \quad (2),$$

where  $u_i$  is the velocity of the incident He beam,  $u_{i\perp}$  is the normal component of  $u_i$ ,  $\theta_i$  is the incident angle of the He beam,  $F_i(u_i)$  and  $G_i(B_1 u_i)$  are the velocity distributions of incident He beam and surface atom, respectively.  $B_1$ ,  $B_2$  and  $G(B_1 u_i)$  are described as follows:

$$B_1 = \frac{1+\mu}{2} \sin\theta_i \cot\theta_f - \frac{1-\mu}{2} \cos\theta_i \quad (3),$$

$$B_2 = \frac{1+\mu}{2} \sin\theta_i \csc^2\theta_f \quad (4),$$

$$G(B_1 u_i) dv_i = \left( \frac{M}{2\pi k_B T_s} \right)^{\frac{1}{2}} \exp\left( -\frac{M}{2k_B T_s} (B_1 u_i)^2 \right) d(B_1 u_i) \quad (5),$$

where  $\mu$  is the mass ratio between the mass of He,  $m$ , and the effective mass of the surface,  $M$ ,  $k_B$  is Boltzmann constant and  $B_1 u_i$  represents the velocity of the surface atom.  $m$ ,  $M$ ,  $E_i$  and  $T_s$  are the set parameters ( $u_i$  is derived from  $E_i$ ). In the calculation,  $F_i(u_i)$  is simply set as  $u_i$  because of the mono-energetic incident He beam used for the measurement as shown in Fig. 1.

As shown in Fig. 3, equation (1) reproduces the experimental results very well. Note that there is no free parameter except for  $\alpha_{HCM}$ ,  $\beta_{HCM}$  and  $M$  in the fitting analysis. The parameters  $\alpha_{HCM}$  and  $\beta_{HCM}$  used for the fitting are plotted in Fig. 4 as a function of the surface temperature. It shows exponential decay of  $\alpha_{HCM}$  with increasing surface temperature. It is due to the Debye-Waller effect as discussed below in detail. On the other hand,  $\beta_{HCM}$  shows little change with the surface temperature, suggesting that the inelastic component of the He from HOPG is well described simply by the hard cube model. The details of the derived effective mass,  $M = 72$  is also described below. In the analysis with equation (1), the first-order diffraction peaks are included into neither elastic nor inelastic scattering component and are not taken into consideration because of its weak intensity as shown in Fig. 2.

### 3.2 Elastic scattering component

The intensity of the He beam specularly scattered from HOPG is plotted as a function of surface temperature in Fig. 5, in which the intensities of the elastic component derived from the fitting analysis are also shown. The intensity of the specularly scattered He beam decreases with increasing surface temperature due to the Debye-Waller effect. As described above, due to the existence of the inelastic scattering component in the intensity of the specular scattering, it is difficult to estimate the surface Debye temperature from raw data. Indeed, the dependence of the specular He intensity on the surface temperature is not plotted by the straight line in the log-scale as shown in Fig. 5.

On the other hand, nearly straight lines are realized in the case of the derived elastic scattering component by the fitting in both analysis method cases as shown in Fig. 5, indicating the expected Debye-Waller plot for a diffraction peak. Thus, on the basis of the following equation [4, 20, 29], the surface Debye temperature,  $\Theta$ , of the HOPG surface can be estimated.

$$I = I_0 \exp\left(-24 \frac{m (E_{\perp} + D) T_s}{M k_B \Theta}\right) \quad (6)$$

where,  $E_{\perp}$  is the normal component of the incident translational energy of He,  $I_0$  is the intensity of the incident He beam and  $D$  is the attractive potential well in the gas-surface potential between He and HOPG. The surface Debye temperature estimated from Fig. 5 by using equation (6) is 586.7 K, where  $D$  is set as the reported value of 15.7 meV in the literature [20]. We have conducted the same measurement and analysis by changing the HOPG sample several times. The derived surface Debye temperature is not always the same value but within  $590 \pm 30$  K. This is in the range of the reported Debye temperatures of the graphite surface; 614 K [30], 530 K [20], and 670 ~ 800 K [31].

The derived surface Debye temperature of the graphite relates to the lattice vibration of the c-axis of graphite, i.e., perpendicular motion of the graphene sheet. This is higher than the surface Debye temperature of most of the transition metal surfaces such as Cu, Ag, Rh, Pt (around ~250 K) [32] possibly due to the specific phonon density of state of graphite [33]; the number of low frequency modes is smaller for graphite than that for metal. However the Debye temperature of the graphite surface is extremely smaller than that of the bulk diamond (bulk Debye temperature of diamond is reported as 2240 K) [33, 34]. The origin of the softness of the graphite compared to the diamond can be attributed to the weaker interaction between graphene layers as reported previously [33]. Indeed, the Debye temperature corresponding to the displacement of carbon atom in graphene is theoretically expected to be over twice as high as that corresponding to the atom displacement normal to the graphene layer [35].

### 3.3 Inelastic scattering component

The derived inelastic scattering components by using equation (1) have physical information concerning the gas-surface interaction potential between He atom with thermal energy and the HOPG surface. As described above, the successful fitting of the experimental results with equation (1) shown in Fig. 3 is only achieved when the effective mass of the surface is set as  $M = 72$  u (six carbon atoms), suggesting that the He atom with thermal energy interact with not only one carbon atom but with at least 6 carbon atoms at the single-collision event. The other choice of the surface effective mass results in a poor reproducibility with experimental results of Fig. 3, that is, the width of the distribution calculated by the hard cube model is quite

different from that of the experimental result. As typical examples, the calculated results of the HCM distribution,  $I_{\text{HCM}}$  of equation (2), at the several effective surface mass are shown in Fig. 6 as functions of the scattering angle and surface temperature. In the case of  $M = 12$  u (one carbon atom), width of all angular intensity distributions are broader than those of experimental results, indicating a larger energy loss of the He due to the multi-phonon creation in the surface at the single collision event. On the other hand, at  $M = 216$  u (18 carbon atoms, i.e. three graphite units) the distribution is sharper than those of experimental results, indicating a smaller energy loss of the He by the single collision event.

The surface effective mass is very often chosen greater than the real mass in many theoretical model analyses [26, 36-52], which is attributed to the corporative motion of the surface atoms [53]. Because the graphite surface consists of  $\pi$  bonded cloud (which originates from the overlap of the lone  $2p_z$  electron orbital of the carbon), the incoming He may interact with this outermost electron clouds due to the Pauli repulsion. As a result, the corporative motion may operate in the graphite to 6 carbon atoms ( $\pi$  bonded cloud). In the case of Xe scattering from HOPG, the effective mass has been reported as  $M = 310$  u [51] which is heavier than the mass derived in our result of  $M = 72$  u. The difference is probably caused by the difference of the size of the incoming atom to the HOPG surface; larger Xe atom interacts with larger number of carbon atoms at the single collision event. Indeed, in the case of smaller atom/molecule scattering such as Ne, Ar and  $\text{CH}_4$ , the effective mass of graphene layer (monolayer graphite) grown on Pt(111) has been estimated as  $M = 72$  u [52], which is the same effective mass with our present result. Beside, in the case of Xe scattering, significant energy loss as much as 80 % of the normal incident energy has been reported to occur by the collision with the HOPG surface due to the heavier mass of Xe, which results in the spatial modulation of few graphene sheets [54]. The collision dynamics with HOPG surface between Xe and He is thus considered to be quite different.

As described in the above, the fitting analysis with equation (1) has successfully reproduced experimentally observed results by using  $M = 72$  u without any inclusion of the corrugation of the interaction potential in the model as shown in Fig. 3. The analysis also does not take into account for the effect of the irregularities of the surface such as step, defect and domain boundary. Generally, the scattering component of He from these irregularities can be described as Cosine distribution in the three-dimensional scattering space. At the in-plane scattering geometry, therefore, the scattering component is considered to be quite smaller than the amount of the direct-inelastic scattering component. Indeed, the angular intensity distribution of He from relatively defective HOPG shows almost the same shape of the distribution with lower intensity, suggesting that the effect of the irregularities of the surface is negligible in our experimentally observed in-plane angular intensity distribution of He, as

expected. The same conclusion has also been reported for the interaction of relatively heavier atom/molecule (Ne, Ar and CH<sub>4</sub>) scattering from graphene layer on Pt(111)[52].

## Conclusion

We have measured angular intensity distribution of He from highly oriented pyrolytic graphite (HOPG). Elastic and inelastic scattering components have been extracted by applying the simple classical binary collision theory of the hard cube model (HCM) to our experimentally observed results. From the extracted elastic scattering component in the scattering distribution, the Debye temperature of the HOPG surface has been derived as  $590 \pm 30$  K. Furthermore, it is also turned out that the best fitting result for the inelastic scattering component is only achieved when the effective mass of the surface is set as  $M = 72$  u (six carbon atoms) in the analysis. The result suggests that, He atom with thermal energy interacts with not only one carbon atom but with at least 6 carbon atoms at the single collision event. In the analysis, the hard cube model well reproduces only for the inelastic scattering component of the experimentally observed angular intensity distribution, that is, the elastic scattering component can not be reproduced simultaneously only by the hard cube model. This suggests that the elastic scattering component in Fig. 3 is composed of the quantum mechanical scattering as a result of the wave nature of He beam while inelastic scattering component is composed of the pure classical scattering. The results in Fig. 3 are thus showing the transition of the scattering event from quantum mechanical scattering to the classical mechanical scattering of He beam from solid surface.

The advantage of the analysis method proposed in this work is its simplicity. It required only one parameter of the effective surface mass to analytically calculate the multi-phonon scattering. The effective mass derived from the analysis represents the property of the He inelastic scattering, i.e. degree of the energy dissipation of colliding He to the surface (the number of interacting atoms on the surface at the single collision event). The method can be applied to even for the scattering results at the corrugated surface by applying the washboard model [55], which is the simple extended theory of the hard cube model. With the demonstrated our new method, therefore, the analysis of He scattering from complicated materials such as organic molecular layer, nano-cluster layer and liquid molecular layer will be possible to delineate the trend of the interaction potential with He and to evaluate the energy dissipation of He to the surface.

## Acknowledgement

We would like to thank Professor Joseph R. Manson (Clemson University) and Dr. Y. Yamada (Univ. Tsukuba) for their fruitful comments. We would also like to thank Professor Maki Kawai (Tokyo University and RIKEN) and Professor Emeritus Shigehiko Yamamoto (University of

Tsukuba) for their support of the apparatus used in this work. We would appreciate the financial support from NEDO (New Energy and Industrial Technology Development).

## References

- [1] J. P. Toennies, *J. Phys. : Condens. Matter.* **5**, A25 (1993).
- [2] K. Heinz, K. Müller, T. Engel, and K.H. Rieder, *Structural Studies of Surfaces* (Springer, Berlin, 1982).
- [3] *Scattering of Thermal Energy Atoms from Disordered Surfaces*, Springer Tracts in Modern Physics, edited by B. Poelsema and G. Comsa (Springer-Verlag, Berlin, 1989).
- [4] G. Scoles, *Atomic and Molecular Beam Methods* (Oxford University Press, New York, 1988), Vol. 1; (1992), Vol. 2.
- [5] W. Kress and F.W. de Wette, *Surface Phonons* (Springer, Berlin, 1991).
- [6] F. Hofmann and J. P. Toennies, *Chem. Rev.* **96**, 1308 (1996).
- [7] D. Farias and K. H. Rieder, *Rep. Prog. Phys.* **61**, 1575 (1998).
- [8] A P Jardine, J Ellis and W Allison, *J. Phys.: Condens. Matter* **14**, 6173 (2002).
- [9] A. P. Graham, *Surf. Sci. Rep.* **49**, 115 (2003).
- [10] R. M. Logan and R. E. Stickney, *J. Chem. Phys.* **44**, 195 (1966).
- [11] B. E. Hayden, *Vibrational Spectroscopy of Molecules on Surfaces*, edited by J. T. Yates, Jr. and T. E. Madey (Plenum, New York, 1987).
- [12] J. R. Manson, *Phys. Rev. B*, **58**, 2253 (1998).
- [13] F. Hofmann, J. P. Toennies and J. R. Manson, *J. Chem. Phys.* **126**, 1234 (1997).
- [14] A. Muis and J. R. Manson, *J. Chem. Phys.* **107**, 1655 (1997).
- [15] R. Brako and D. M. Newns, *Phys. Rev. Lett.* **48**, 1859 (1982); *Surf. Sci.*, **123**, 439 (1982).
- [16] G. Boato, P. Cantini and R. Tatarek, *Phys. Rev. Lett.* **40**, 887 (1978).
- [17] W. E. Carlos and M. W. Cole, *Surf. Sci.* **91**, 339 (1980).
- [18] P. Cantini and R. Tatarek, *Phys. Rev. B* **23**, 3030 (1981).
- [19] J. Hutchison and V. Celli, *Surf. Sci.* **93**, 263 (1980).
- [20] G. Boato, P. Cantini, C. Salvo, R. Tatarek and S. Terreni, *Surf. Sci.* **114**, 485 (1982).
- [21] G. Benedek, G. Brusdeylins, C. Heimlich, J. P. Toennies and U. Valbusa, *Surf. Sci.* **178**, 545 (1986).
- [22] H. Jonsson and J. H. Weare, *J. Chem. Phys.* **86**, 3711 (1987).
- [23] J. A. Barker and D. J. Auerbach, *Surf. Sci. Rep.* **4**, 1 (1985).
- [24] C.T. Rettner and M.N.R. Ashfold, *Dynamics of Gas-Surface Interactions* (The Royal Society of Chemistry, London, 1991).
- [25] C. T. Rettner, D. J. Auerbach, J. C. Tully, and A. W. Kleyn, *J. Phys. Chem.* **100**, 13021 (1996).

- [26] T. Kondo, H. S. Kato, T. Yamada, S. Yamamoto, and M. Kawai, *Eur. Phys. J. D* **38**, 129 (2006).
- [27] T. Kondo, H. S. Kato, M. Bonn, and M. Kawai, *J. Chem. Phys.* **127**, 094703 (2007)
- [28] S. Yamamoto and R.E. Stickney. *J. Chem. Phys.* **53**, 1594 (1970).
- [29] J. L. Beeby, *J. Phys. C* **4**, L359 (1971).
- [30] R. W. Gurney, *Phys. Rev.* **88**, 465 (1952).
- [31] J. P. Biberian, M. Bienfait and J. B. Theeten, *Acta Cryst. A* **29**, 221 (1977).
- [32] F. Hofmann, J. P. Toennies and J. R. Manson, *J. Chem. Phys.* **101**, 10155 (1994).
- [33] T. Tohei, A. Kuwabara, F. Oba, I. Tanaka, *Phys. Rev. B*, **73**, 064304 (2006).
- [34] A. Migliori, H. Ledbetter, R. G. Leisure, C. Pantea and J. B. Betts, *J. Appl. Phys.* **104**, 053512 (2008).
- [35] J. Krumhansl, H. Brook, *J. Chem. Phys.* **21**, 1663 (1953).
- [36] I. Moroz and J. R. Manson, *Phys. Rev. B* **69**, 205406 (2004).
- [37] I. Moroz, H. Ambaya, and J. R. Manson, *J. Phys.: Condens. Matter* **16**, S2953 (2004).
- [38] I. Moroz and J. R. Manson, *Phys. Rev. B* **71**, 113405 (2005).
- [39] T. Kondo, T. Tomii, and S. Yamamoto, *Chem. Phys.* **320**, 140(2006).
- [40] D. Velic and R. J. Levis, *Chem. Phys. Lett.* **269**, 59 (1997).
- [41] T. Kondo, R. Okada, D. Mori, and S. Yamamoto, *Surf. Sci.* **566–568**, 1153 (2004).
- [42] T. Kondo, D. Mori, R. Okada, and S. Yamamoto, *Jpn. J. Appl. Phys.* **43**, 1104 (2004).
- [43] T. Kondo, T. Tomii, S. Yagyu, and S. Yamamoto, *J. Vac. Sci. Technol. A* **19**, 2468 (2001).
- [44] G. Armand, J. Lapujoulade, and Y. Lejay, *Surf. Sci.* **63**, 143 (1977).
- [45] C. R. Arumainayagam, M. C. McMaster, G. R. Schoofs, and R. J. Madix, *Surf. Sci.* **222**, 213 (1989).
- [46] S. Yagyu, F. Murakami, Y. Kino, and S. Yamamoto, *Jpn. J. Appl. Phys.* **37**, 2642 (1998).
- [47] A. C. Wight and R. E. Miller, *J. Chem. Phys.* **109**, 1976 (1998).
- [48] T. Tomii, T. Kondo, T. Hiraoka, T. Ikeuchi, S. Yagyu, and S. Yamamoto, *J. Chem. Phys.* **112**, 9052 (2000).
- [49] T. Kondo, T. Tomii, T. Hiraoka, T. Ikeuchi, S. Yagyu, and S. Yamamoto, *J. Chem. Phys.* **112**, 9940 (2000).
- [50] B. Berenbak, S. Zboray, B. Riedmuller, D. C. Papageorgopoulos, S. Stolteb, and A. W. Kleyn, *Phys. Chem. Chem. Phys.* **4**, 68 (2002).
- [51] Y. Watanabe, H. Yamaguchi, M. Hashinokuchi, K. Sawabe, S. Maruyama, Y. Matsumoto, K. Shobatake, *Euro. Phys. J. D* **38**, 103 (2006).
- [52] T. Kondo, D. Mori, R. Okada, M. Sasaki and S. Yamamoto, *J. Chem. Phys.* **123**, 114712 (2005).
- [53] E. K. Grimmelmann, J. C. Tully, and M. J. Cardillo, *J. Chem. Phys.* **72**, 1039 (1980).

[54] Y. Watanabe, H. Yamaguchi, M. Hashinokuchi, K. Sawabe, S. Maruyama, Y. Matsumoto, K. Shobatake, Chem. Phys. Lett. **413**, 331 (2005).

[55] J. C. Tully, J. Chem. Phys, **92**, 680 (1990).

### Figure captions

#### Fig. 1

Time-of-flight distribution of incident He. The nozzle temperature  $T_n$ , the pressure inside the nozzle  $P_0$ , flight pass length  $L$ , nozzle-skimmer distance  $d$ , and the nozzle pinhole diameter  $\phi_n$  are labeled in the figure. The fitting result used for the deconvolution of the chopper gate-function is also shown in the figure by the blue solid curve [15].

#### Fig. 2

The angular intensity distribution of He scattered from the HOPG surface.

#### Fig. 3

The surface temperature dependence of the angular intensity distribution of He scattered from the HOPG surface. The results of the analytical fitting (see text) are also shown in the figure. ES+HCM (elastic scattering + hard cube model) represent equation (1).

#### Fig.4

The component factors used for the calculation with equation (1),  $\alpha_{HCM}$  and  $\beta_{HCM}$ , are shown as a function of the surface temperature.

#### Fig. 5

The surface temperature dependence of the specular intensity of He scattered from HOPG. The experimental results are plotted by the solid circle. The solid triangle represents the intensity of

the elastic scattering component derived by the analysis using equation (1).

**Fig. 6**

The hard cube model calculation. The distribution is calculated by using equation (2). The calculations are conducted by set the parameters as  $m = 4$  and  $E_i = 63$  meV. The effective mass of the surface  $M$  and the surface temperature  $T_s$  are varied as shown in the figure. The arrows are represents the order of the  $T_s$ , i.e. 150 K, 200 K, 250 K, 300 K, 350 K and 400K.

**Fig. 1**

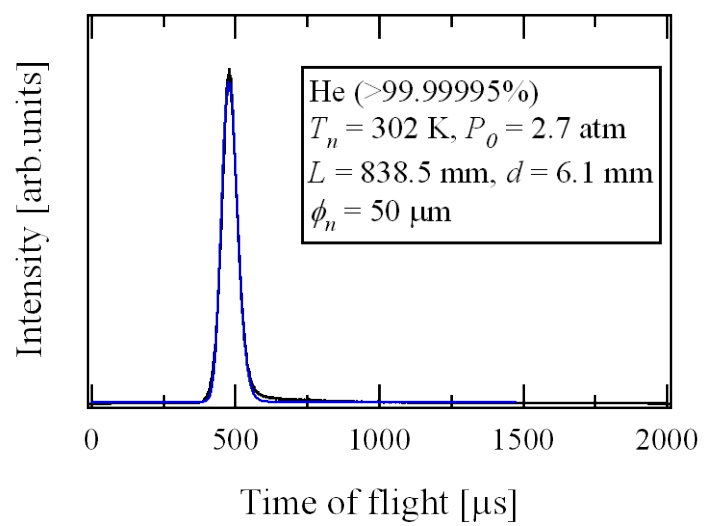


**Fig. 2**

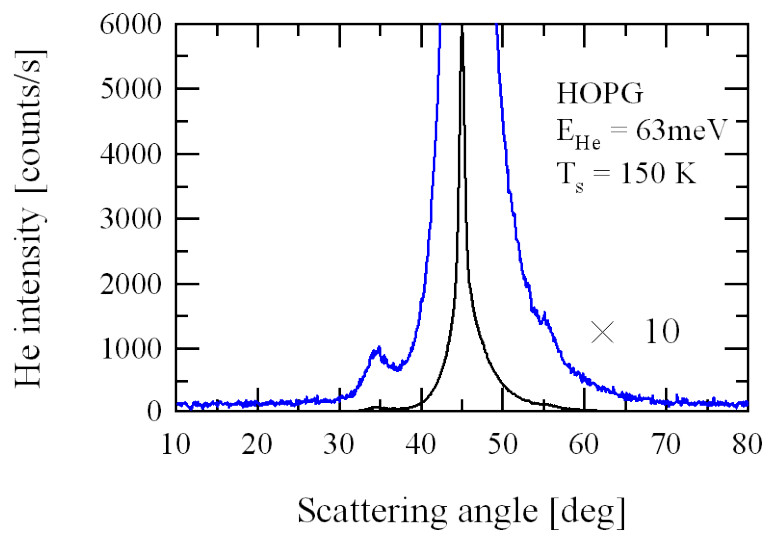
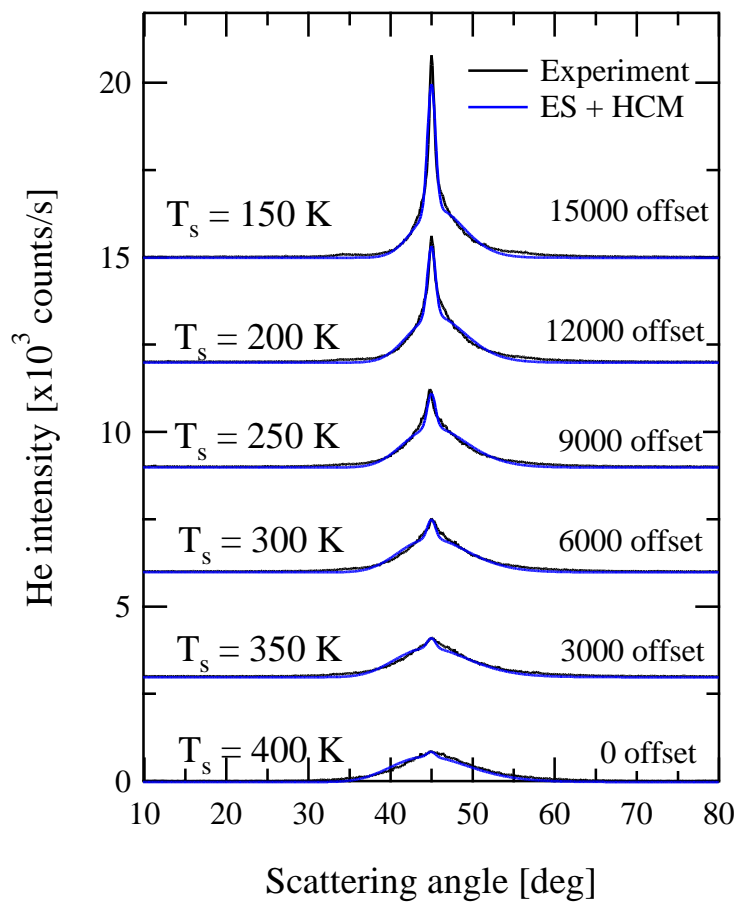


Fig. 3



**Fig. 4**

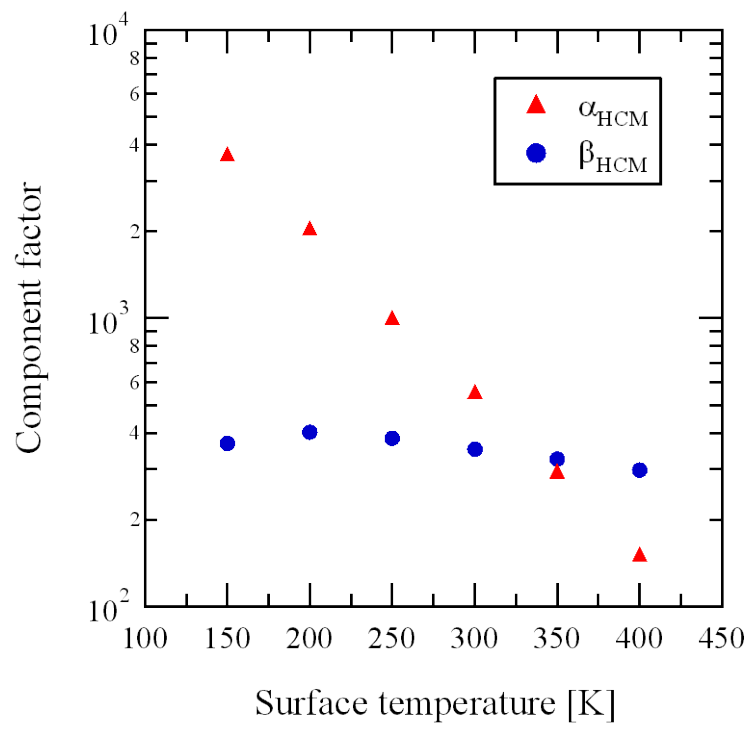
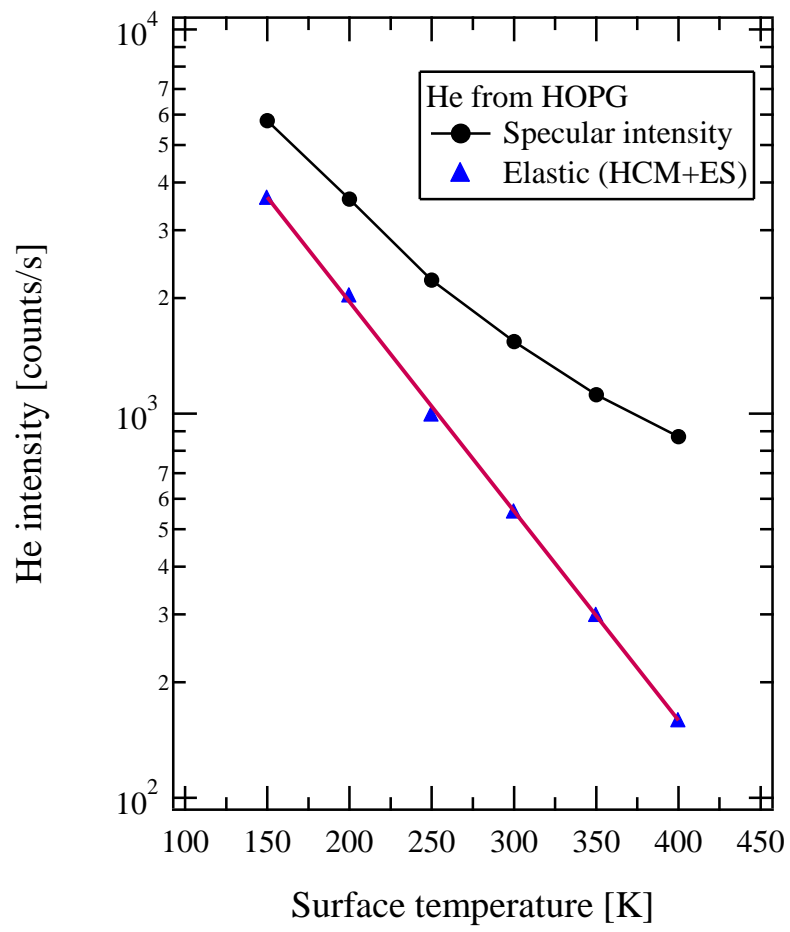


Fig. 5



**Fig. 6**

